American-Eurasian J. Agric. & Environ. Sci., 3 (3): 498-505, 2008
ISSN 1818-6769

A Two Dimensional Finite Element Analysis of a Plane Tillage Tool in Soil Using a Non-linear Elasto-Plastic Model

[1]Shahab Davoudi, [1]Reza Alimardani, [1]Alireza Keyhani and [2]Reza Atarnejad

[1]Department of Agricultural Machinery Engineering,
Faculty of Biosystems Engineering, University of Tehran, Karaj, Iran
[2]Faculty of Civil Engineering, University of Tehran, Iran

Abstract: A numerical model of contact between a tillage tool and soil and their interaction is a useful and powerful method for analyzing and understanding the phenomena and optimization in design process. In this task, a 2-D non-linear numerical finite element model in the form of plain strain was developed to analyze the behavior of tillage tool moving in a bulk of soil, soil failures and force reactions. The soil was modeled assuming it is completely homogenous, based on Drucker-Prager's elastic-perfectly plastic model. Contact elements were used to make a better connection between tillage tool surface and soil, to obtain a better soil elements movement on the blade surface, using Coulomb's theorem. The finding of this task is a model which predicts the soil movements and soil failure surfaces due to simple tillage operation, elastic and plastic stress distribution in soil, hard pan formation area, stress distribution on the blade of tillage tool and required draft force needed for blade movement in the soil. This model was compared to other models and experimental data and showed a good agreement in the prediction trends among them. The comparis on verified the model, so the model can be used to analyze tillage tool-soil interaction to predict required draft forces as well as design and optimization of tillage tools.

Key words: Plane blade tillage tool . Elasto-plastic model . draft . stress distribution . finite element

INTRODUCTION

More than 50% of required energy in agricultural activities is consumed by tillage operation. This high demand of energy is because of the work done on a great amount of soil volume and also the absence of data and knowledge. Tillage and soil-tool interaction is not a quantitive-base science yet and many of its concepts are represented qualitatively. Although both analytic and numerical methods are used to study soil cutting process and soil-tool interaction, numerical methods, including finite element method, are more helpful in understanding and describing the subject. This method can be used to predict stress distribution in soil, soil deformation and acting forces on tools. Soil mechanical behavior and soil-tool reactions are two main subjects being considered in finite element analysis of soil-tool interaction. Soil mechanical behavior is usually being simulated by a non-linear model or elastic-perfectly plastic model [1]. Soil-tool reaction is being declared by friction model or friction with cohesion model [2].

Researchers have used different models to simulate soil bulk and the contact between soil and tool. However, in analysis with non-linear elastic model, Duncan-Chang's hyperbolic model and in analysis with elastic-perfectly plastic model, Drucker-Prager's elastic-perfectly plastic model are used. The advantage of hyperbolic elastic model is its simplicity, but the soil plastic behavior is not being considered.

Asaf *et al.* [3] during their research for defining required parameters for soil simulation found that it is required to use elasto-plastic relationship to increase accuracy and to minimize error to less than 15%.

Chi and Kushwaha [4] developed a 3-D model to study soil failure with a narrow tillage tool. The mechanics of soil elements were modeled using Duncan-Chang's elastic model and the soil-tool interaction was simulated by considering friction as well. The result of their task included soil forces, soil failure regions, displacement field and stress distribution on the tool. The model was verified in laboratory using a soil bin.

Araya and Gao [5] used ADINA software package and assumed soil mechanical behavior to be elastic-perfectly plastic in the form of Drucker-Prager's theorem to develop a model for soil failure with the movement of a narrow subsoiler blade.

Corresponding Author: Shahab Davoudi, Department of Agricultural Machinery Engineering, Faculty of Biosystems Engineering, University of Tehran, Karaj, Iran

Abo-Elnor *et al*. [6] simulated soil-narrow blade interaction using ABAQUS software package and assuming elastic soil behavior. They delineated vertical and horizontal soil failure surfaces at first to overcome the solution convergence problem caused due to large blade displacement. They verified the model by finding the maximum shear stress areas in the soil after running the software and comparing it with the predefined soil failure surfaces.

The objective of this study was to develop a finite element model using ANSYS software to predict and determine the draft force required for a moving plane tillage blade in the soil. The model should be capable of predicting the required tillage tools draft forces. In this work, soil was considered to be elastic-perfectly plastic and Drucker-Prager's criterion was used. The soil failure surfaces were not predefined and the model could locate soil failure surfaces during the convergence process.

MATERIALS AND METHODS

Elastic-perfectly plastic theorem: Soil elastic-perfectly plastic behavior is described in two stages. In Fig. 1 soil behavior is assumed pure elastic when $0=\varepsilon=\varepsilon_0$ and pure plastic when $\varepsilon_0=\varepsilon$.

The stress-strain relationship on the domains of said definition is shown by Eq. 1.

$$\sigma = \begin{cases} k_1 e & 0 \le e \le e_0 \\ k_2 & e_0 \le e \end{cases} \quad (1)$$

where σ is the axial stress, ε is the axial strain, ε_0 is the critical strain at the point where plasticity begins, k_1 and k_2 are the parameters and

$$\sigma_Y = f(\sigma_m)$$
$$\sigma_m = \frac{1}{3}(\sigma_x + \sigma_y + \sigma_z)$$

where σ_Y is the yield stress and σ_m is the mean principal stress.

Agricultural soils are subject to plastic deformation after a certain external load. Hence, the total strain can be divided into elastic and plastic strains as:

$$d\varepsilon = d\varepsilon^e + d\varepsilon^p \quad (2)$$

where $d\varepsilon$ is the incremental total strain, $d\varepsilon^e$ is the incremental elastic strain and $d\varepsilon^p$ is the incremental plastic strain.

Based on Hook's elastic law, the incremental stress is proportional to incremental strain [7].

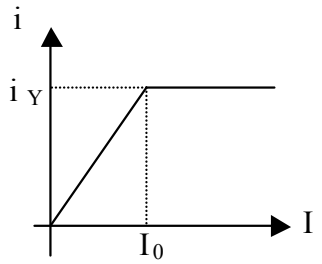

Fig. 1: Stress-strain behaviour of elastic-perfectly plastic soil

$$ds = D^e de^e = D^e (de - de^p) \quad (3)$$

where $d\sigma$ is the incremental stress, D^e is the soil elastic matrix that is a function of elastic modulus (E) and Poission's ratio (ν). Elastic modulus and Poission's ratio are both elastic parameters which can be calculated using the standard tri-axial test data.

The classic theorem of plasticity states that the incremental plastic strains are proportional to the derivation of the yield function to the incremental strain. The yield function of an elastic-perfectly plastic material is a fixed surface in the principal stress space (Fig. 2). The state of stress inside the yield surface describes the elastic state in which deformations are completely reversible. When the stress locations reach yield surface, plastic strain occurs and hence both reversible and permanent deformation are formed.

In order to define the plastic strain, another function named potential plastic function is considered. The potential plastic function is a surface in the principal stress space similar to the yield surface. The incremental plastic strain is defined as a function of the potential plastic function:

$$de^p = \lambda \frac{\partial g}{\partial s} \quad (4)$$

where g is the potential plastic function and λ is the plastic multiplier. As long as the location of stress is inside the space bounded by the yield surface, the plastic multiplier is equal to zero. As soon as the location of stress reaches the yield surface and plastic strain occurs the plastic multiplier becomes greater than zero. This late situation is called elastoplastic phase. So substituting Eq. 4 into Eq. 3 yields:

$$ds = D^e de - \lambda D^e \frac{\partial g}{\partial s} \quad (5)$$

In the Drucker-Prager's model, it was assumed that the potential plastic function and the yield function are the same, that is f = g [8].

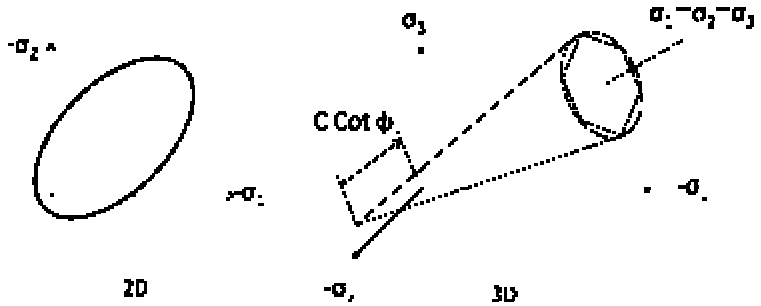

Fig. 2: Drucker-Prager's yield surface in 2D space (left) and 3D space (right)

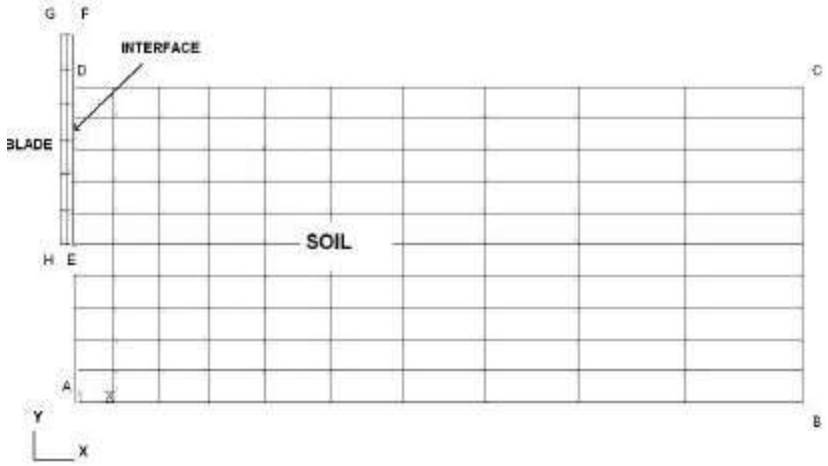

Fig. 3: The 2D meshing of soil-blade and boundary conditions

Yield function: Drucker and Prager introduced a yield function for the elastic-perfectly plastic model in the 3D space of principal stresses based on Mohr-Coulomb's yield function in the 3D space of principal stresses as follow:

$$f(\sigma) = 3\alpha\sigma_m + J_2^{1/2} - k = 0$$

where $f(\sigma)$ is the yield function, J_2 is the second deviatoric stress invariant and k is a material parameter; each defined as follow:

$$\sigma_m = \frac{1}{3} I_1 \quad (7)$$

$$I_1 = \sigma_x + \sigma_y + \sigma_z \quad (8)$$

$$J_2 = \frac{1}{2}\left[\begin{array}{r}(\sigma_x - \sigma_m)^2 + (\sigma_y - \sigma_m)^2 \\ + (\sigma_z - \sigma_m)^2\end{array}\right] + \tau_{xy}^2 + \tau_{yz}^2 + \tau_{xz}^2 \quad (9)$$

$$\alpha = \frac{2\sin\phi}{\sqrt{3}(\sin\phi)} \quad (10)$$

$$k = \frac{6c\cos\phi}{\sqrt{3}(3 - \sin\phi)} \quad (11)$$

where I_1 is the first stress invariant, σ_x, σ_y and σ_z are respectively the stresses in the x,y and z direction; t_{xy}, t_{yz} and t_{zx} are the shear stresses on xy, yz and xz planes, respectively, c is the soil cohesion and ϕ is the soil internal friction.

Model development: Finite element model of soil-blade interaction was developed and coded using ANSYS software V10. The tool was assumed as a wide blade with width to depth ratio of greater than 2. In this kind of blades soil is moved only forward and upward and little end effects are neglected [9]. In this case, it is possible to run a 2D analysis in the form of plane strain. A 2D finite element meshing forming a rectangular (ABCD) by the length of 60 cm and depth of 24 cm using rectangular 4-node elements was created to model the soil (Fig. 3). The length of this area was divided into 10 segments with the numerical ratio of 1 to 3. So although the total number of elements reduced, the elements adjacent to the blade were smaller in size,

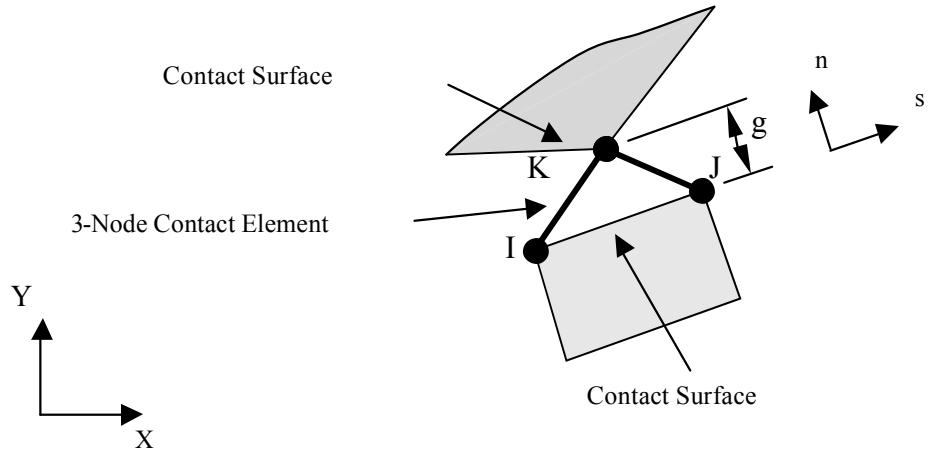

Fig. 4. The geometry of 3-node contact element

providing more accurate results. The depth was also divided into 10 equal segments. A total numbers of 100 soil elements was developed.

The blade was created by 2D, 4-node rectangular elements leading to a rectangle with the width of 1 cm and length of 12 cm. The 10 cm length of the blade was considered to be in the soil and 2 cm out of the soil surface. The outer part was used for applying the force to the blade and also acting as an obstacle causing the soil to move upward after failure.

The boundary conditions were applied by restricting the movement on the bottom (AB) and on the right side of the soil model (far away from the blade). The assumption was such that two boundaries are distant enough from the blade that no displacement would occur as a result of blade movement. It was assumed that the upper surface (CD) of the soil and the surface in contact to the blade (AD) had no restrictions for movement if needed. To enforce the blade movement in the soil, a predefined horizontal displacement of 4 cm in the direction of the x-axis was applied on all nodes on the surface EH of the blade. This displacement was added to the system in 58 steps. The vertical movement of the blade was also restricted by limiting its degree of freedom parallel to the y-axis direction.

Material properties: The soil elasto-plastic behavior is completely defined by cohesion, internal angle of friction, modulus of elasticity and Poisson's ratio [10]. The properties of soil, blade and contacting surface of soil-blade is shown in Table 1. These data were used as input data for the model. The soil-blade adhesion was implicitly defined by the external angle of friction in the model.

Contact elements and friction: To study the reactions and slip between soil and the blade, coulomb's friction criterion was used. Plane 3-node elements were considered as connecting elements between the two surfaces [11]. The contact element is shown in Fig. 4.

Table 1: Soil and contacting surface of soil-blade properties

Amount	Properties
Soil material properties	
Density (kg m^{-3})	1800
Cohesion (kPa)	15000
Internal friction angle (degree)	30
Poisson's Ratio	0.36
Modulus of elasticity (kPa)	8000
Blade material properties	
Density (kg m^{-3})	8000
Poisson's Ratio	0.3
Modulus of elasticity (kPa)	800000
Contacting surface properties	
Soil-blade angle of friction (degree)	20

The normal forces acting on the contact surfaces of two bodies is given by Eq. 12.

$$f_n = \begin{cases} k_n g & g \le 0 \\ 0 & g > 0 \end{cases} \quad (12)$$

where g is the distance between the two contact surfaces which determines contact establishment and k_n are the contact stiffness.

The tangential force reactions acting on the plane of contact surfaces is given by Eq. 13:

$$f_s = \begin{cases} k_t u_s^e & \text{If sticking} \\ \hat{f}_s & \text{If sliding} \end{cases}$$

where k_t is the cohesive stiffness, u_s^e is the elastic tangential displacement and $\hat{f}_s$ is the cohesive force limit in Coulomb's friction model.

In assembling a symmetric matrix during the solution phase, the number of contact elements was considered as twice as common. So a group of elements had 2 nodes on the blade surface and one node on the soil surface and another group had contrary nodes. These elements were so aligned to contact all the nodes on the soil surface to all the nodes on the blade surface. Although the numbers of elements are increased, there was no problem in detachment of soil-blade during the analysis process. A total number of 72 contact elements was developed.

Model coding and run: The ANSYS code was consisted of 202 lines. The model was run on a Windows XP machine with a 1.6 GHz Pentium 4 CPU, 512 MB of RAM and 1 GB swap memory. The average consumed CPU time including the pre and post processes was 150 seconds; different runs with different memory management changed the consumed time by about 10 percent.

RESULTS AND DISCUSSIONS

The results of the developed model provided following information regarding the blade forces, soil deformation, soil displacement field, soil stresses, blade stresses.

Blade forces: Using the plane strain assumption, the forces presented here were calculated for the unit width of the blade. Also recalling that the blade width should be at least twice the working depth, the minimum working width of the blade would be 20 cm; in this case to compute the corresponding forces, the results should be multiplied by a factor of 20.

The draft and vertical forces acting on the blade are shown in Fig. 5. These forces are the sum of all horizontal and vertical reactions on the blade nodes after the predefined displacement were applied, respectively. This sum was calculated during each step of applying the displacements. The draft force increased from zero at start to a maximum of 13.69 kN at displacement equal to 1.13 cm. Then, this amount was reduced 20.4 percent and became 10.9 kN. The reason for this reduction can be related to the soil failure formation, leading to less force required to continue the movement.

The experiments conducted to verify Shmulevich *et al*. [12] model showed that at the beginning of movement the draft force increased to about 17 N and after a 25 mm displacement it was reduced to 13 N. The amount of reduction in their experiments was 23.5 percent. Comparing the results presented by this work and Shmulevich's measurements, a good agreement in the trends is observed and the maximum difference in estimating the reduction of draft force was found to be 3.1 percent. One of the reasons for this difference could be the soil parameters, though there were good agreements between two the models and experimental data.

The tendency of vertical force at start was to move the blade upward to push it out of the soil. However,

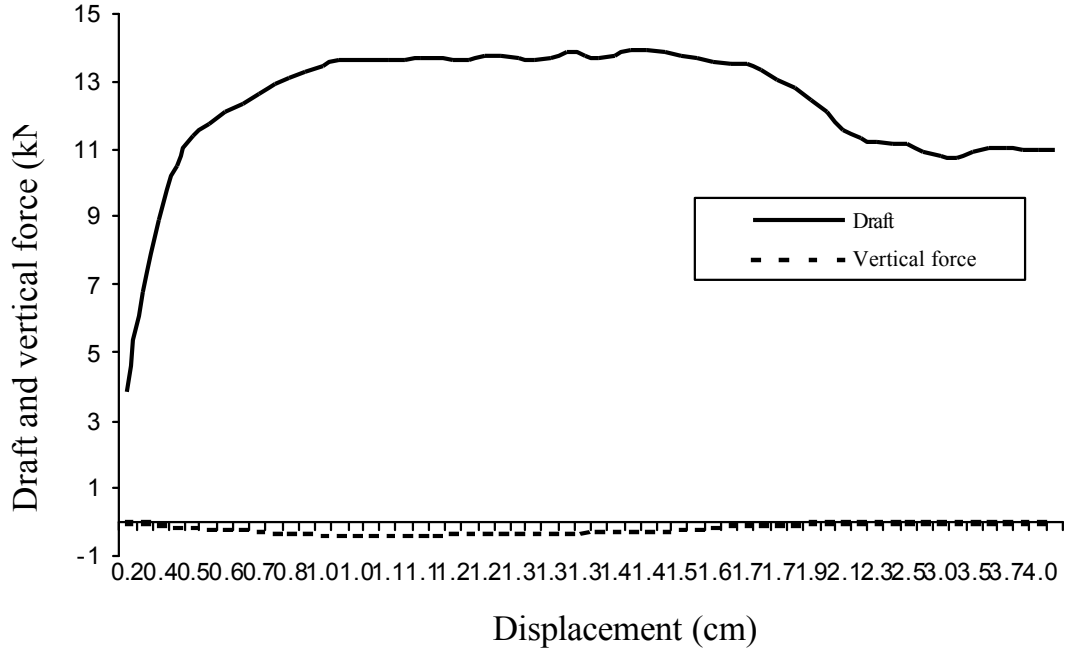

Fig. 5: Draft force (up) and vertical force (down) acting on the blade vs. displacement

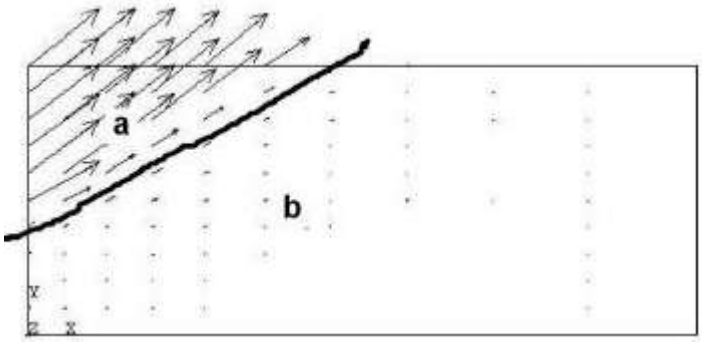

Fig. 6: Soil node displacement vectors

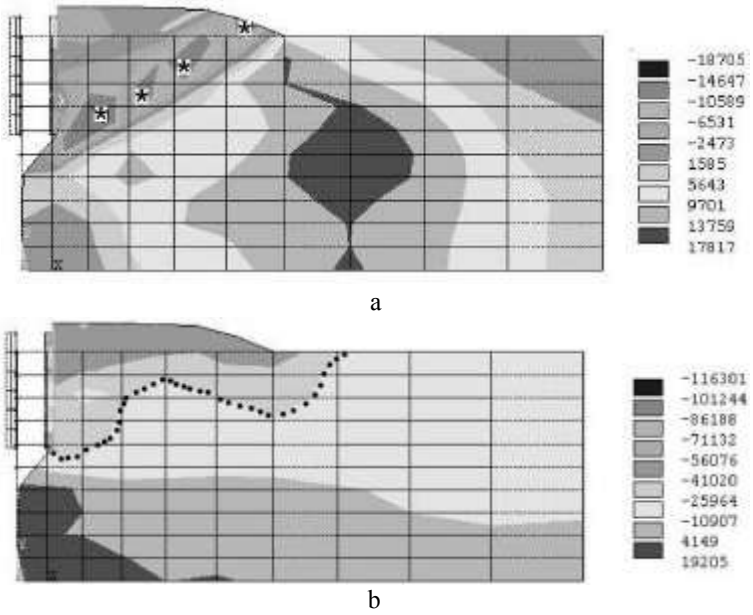

Fig. 7: a) Shear stress in the soil. The maximum absolute shear stress value is shown by "*". b) Minor principal stresses. The failure edge due to tensile is shown by "…"

after a displacement of about 2 cm the amount of this force was reduced. The maximum vertical force was about 400 N when the displacement was 1 cm. The cause of the initial upward driven of the blade can be related to the frictional forces acting on the blade after soil particles were moving upward. The soil particles displacement vectors (Fig. 6) show that the soil displacements beneath the blade tip and adjacent to the blade have upward components. Shmulevich *et al.* [12] model also predicted the same behavior. Their experiments verified this phenomenon as well. The reduction in the vertical force can be caused by loosing the soil in the vicinity of the blade after a given displacement.

Soil deformation: The displacement vectors on soil nodes are shown in Fig. 6. Almost all the displacement directions were up-right (in the direction of blade movement) oriented and the maximum amount of displacement was found to be 4.9 cm and related to the two upper nodes in adjacent to the blade. Considering Fig. 6, the soil bulk can be divided into two regions. The region adjacent to the blade with a considerable amount of displacement (a) and the region with little or no displacement (b). This soil behavior can be explained by Fig. 7a and 7b that where the soil being cut along the line of maximum shear stresses and separated into two distinguished regions a and b (Fig. 6), as the blade movement causes region a to slide over region *b*.

Soil stresses: The shear stress in the soil at maximum displacement is shown in Fig. 7. The maximum shear stresses are along a crescent shape line that join the

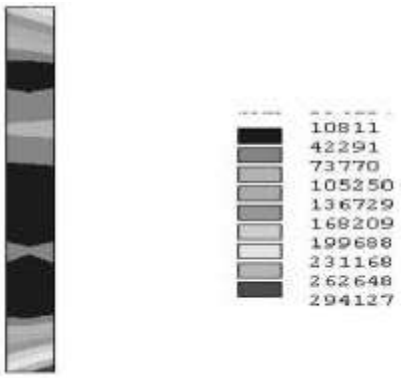

Fig. 8: Von-Misses stress distribution on the blade

blade bottom end to the soil surface by a 25 degree inclined path. These sections are shown by "*". The absolute value of these stresses was 18.7 kPa.

Figure 7b shows minor principal stresses. The almost horizontal contour line passing the bottom end of the blade is the edge between negative minor principal stresses (up) and positive minor principal stresses (down). Inside the region of negative minor principal stresses, soil is under tension and there is a possibility of tensile failure. However, this failure occurs on the edge shown with "…" and the amount of stress is -25.9 kPa, since the amount of minor principal stresses on the corresponding nodes are more than the soil cohesion [13]. The edge of positive and negative minor principal stresses that passes below the blade tip represents a region that the soil beneath it is under positive stress (compression) and thus hardpan can be formed.

Blade stresses: Figure 8 shows Von-Misses stress distribution on the blade surface when it reaches to its utmost movement. The maximum Von-Misses stress was obtained on the bottom-right node on the blade (point E in Fig. 3 and Fig. 8) and its amount was found to be 294.1 kPa. As this point coincide with a node in soil where the failure starts, this was already predictable. The amount of stress is being reduced as moving upward on the blade. But at the upper end (point G) its value is increased again. This can be due to the fact that the soil is moved on the blade upward to resist against the blade displacement.

CONCLUSIONS

The blade movement in the soil considered in this study resulted in the computation of the draft force to be 10.9 kN per unit width after a 2 cm displacement. Also the up-warded vertical force acting on the blade from the soil was reached to a maximum of 400 N and then reduced after more displacement. Results were comparable with those of other studies and experimental data with good agreements.

The model predicts failure points in the soil by comparing minor principal stresses on nodes with the soil cohesion. Checking the soil stresses and displacements showed that the soil failure started from the bottom end of the blade and reached the soil surface on a 25 degree inclined edge. This path divided the soil into two regions. The study of soil displacement also showed that the soil bulk over this edge slide upward and forward on the soil bulk beneath the edge. The largest displacement vectors belonged to the soil particles adjacent to the upper part of the blade. Also, the location where hardpan could be formed was estimated to be in the region with compressive stresses.

Some stresses are applied on the blade due to its movement in the soil. The study of stress distribution on the blade showed that the maximum amount of stress was occurred on the bottom right end point which was responsible for cutting the soil. The state of stress distribution is helpful to locate the points of excessive wear as well as to design for maximum strenght.

REFERENCES

1. Mouazen, A.M. and M. Nemenyi, 1998. A review of the finite element modelling techniques of soil tillage. Math. Comp. Simul., 48: 23-32.
2. Shen, J. and R.L. Kushwaha, 1998. Soil-Machine Interaction: A Finite Element Perspective. Marcel Dekker, Inc. New York, USA.
3. Asaf, Z., D. Rubinstein and I. Shmulevich, 2007. Determination of discrete element model parameters required for soil tillage. Soil and Tillage Res., 92: 227-242.
4. Chi, L. and R.L. Kushwaha, 1990. A non-linear 3-D finite element analysis of soil failure with tillage tool. J. Terramech.,. 27: 343-366.
5. Araya, K. and R. Gao, 1995. A non-linear three-dimentional finite element analysis of subsoiler cutting with pressurized air injection. J. Agric. Eng. Res., 61: 115-128.
6. Abo-Elnor, M., R. Hamilton and J.T. Boyle, 2004. Simulation of soil-blade interaction for sandy soil using advanced 3D finite element analysis. Soil and Tillage Res., 75: 61-73.
7. Taiebat, M. and Y. Bao, 2005. A critical state two-surface plasticity model. Project Report ECI 285. Department of Civil & Environmental Engineering. University of California, Davis, USA.
8. Mouazen, A.M. and M. Nemenyi, 1999. Finite element analysis of subsoiler cutting in non-homogenous sandy loam soil. Soil and Tillage Res., 51: 1-15.

9. Godwin, R.J. and G. Spoor, 1977. Soil failure with narrow tines. J. Agric. Eng. Res., 22: 213-228.
10. Mouazen, A.M. and H. Ramon, 2002. A numerical-statistical hybrid modeling scheme for evaluation of draught requirements of a subsoiler cutting a sandy loam soil, as affected by moisture content, bulk density and depth. Soil and Tillage Res., 63: 155-165.
12. Shmulevich, I., Z. Asaf and D. Rubinstein, 2007. Interaction between soil and a wide cutting blade using the discrete element method, Soil and Tillage Research. (In Press) doi:10.1016/j.still.2007.08.009.
13. Ibarra, S.Y., E. McKyes and R.S. Broughton, 2005. A model of stress distribution and cracking in cohesive soils produced by simple tillage implements. J. Terramechanics, 42: 115-139.